Enhancing intermediate band solar cell performances through quantum engineering of dot states by droplet epitaxy

Received: 16 September 2022 | Revised: 23 December 2022 | Accepted: 23 January 2023

DOI: 10.1002/pip.3672

RESEARCH ARTICLE

PROGRESS IN PHOTOVOLTAICS WILEY

Enhancing intermediate band solar cell performances through quantum engineering of dot states by droplet epitaxy

Andrea Scaccabarozzi[1,2] | Stefano Vichi[1] | Sergio Bietti[1] | Federico Cesura[1] | Timo Aho[3,4] | Mircea Guina[2] | Federica Cappelluti[5] | Maurizio Acciarri[1] | Stefano Sanguinetti[1]

[1]L-NESS and Dipartimento di Scienza dei Materiali, Università di Milano-Bicocca, Milan, Italy

[2]Politecnico di Milano, Milan, Italy

[3]Tampere University, Tampere, Finland

[4]Modulight Corporation, Tampere, Finland

[5]Department of Electronics and Telecommunications, Politecnico di Torino, Torino, Italy

Correspondence
Stefano Vichi, L-NESS and Dipartimento di Scienza dei Materiali, Università di Milano-Bicocca, Milano, Italy.
Email: stefano.vichi@unimib.it

Present addresses
Andrea Scaccabarozzi, Politecnico di Milano, Milan, Italy; and Timo Aho, Modulight Corporation, Tampere, Finland.

Funding information
European Union Horizon 2020 project TFQD, Grant/Award Number: 687253

Abstract

We report the effect of the quantum dot aspect ratio on the sub-gap absorption properties of GaAs/AlGaAs quantum dot intermediate band solar cells. We have grown AlGaAs solar cells containing GaAs quantum dots made by droplet epitaxy. This technique allows the realization of strain-free nanostructures with lattice matched materials, enabling the possibility to tune the size, shape, and aspect ratio to engineer the optical and electrical properties of devices. Intermediate band solar cells have been grown with different dot aspect ratio, thus tuning the energy levels of the intermediate band. Here, we show how it is possible to tune the sub-gap absorption spectrum and the extraction of charge carriers from the intermediate band states by simply changing the aspect ratio of the dots. The tradeoff between thermal and optical extraction is in fact fundamental for the correct functioning of the intermediate band solar cells. The combination of the two effects makes the photonic extraction mechanism from the quantum dots increasingly dominant at room temperature, allowing for a reduction of the open circuit voltage of only 14 mV, compared to the reference cell.

KEYWORDS
droplet epitaxy, III–V semiconductors, intermediate band solar cell, quantum dot

1 | INTRODUCTION

Intermediate band (IB) solar cells have been proposed[1,2] as a way to overcome one of the fundamental limitations intrinsic to the generation of an electric current by absorption of light in semiconductors, that is, the threshold energy that photons must have in order to generate electron–hole pairs in semiconductors. The concept is basically that if a half-full energy band (the IB) is present in the middle of the bandgap of a semiconductor, sub-gap optical transitions involving the IB are enabled, thus increasing the generation of carriers in a solar cell. Radiative only recombination effects should not be detrimental for device performance if the system can be described by three independent quasi-Fermi levels, for conduction, valence, and IB, respectively.[3] If these conditions are fulfilled, the short-circuit current of the device will increase, and the open circuit voltage will remain the same of a device with the same bandgap, thus leading to a net increase of efficiency, that has been demonstrated to reach 63% under maximal concentration.[1,2]

The research on IB photovoltaics has achieved a few years ago the important milestone of the demonstration of the two-photon

absorption effect in quantum dot (QD) solar cells,[4] that is, the key operating principle of IB photovoltaics. However, to the knowledge of the authors, despite many research groups reported an increase in photocurrent due to the extension of the absorption coefficient to sub-gap energies,[2,5–8] nobody has demonstrated that the open circuit voltage is preserved at room temperature for a device operating under IB conditions. The presence of defects in strained structures, like the well-studied InAs/GaAs materials system, leads to pinning of the Fermi level at the defects states,[9] thus decreasing the open circuit voltage in nanostructured devices. Even in an ideal material without defects, thermal coupling between QD confined states and transport bands causes open circuit voltage reduction.[10,11] Devices with good performance have been realized, but the existence of three independent quasi-Fermi levels, as required by the IB theory, is not totally clarified in the literature.[12–14]

Most of the research in this field is devoted to the investigation of InAs/GaAs QD solar cells[4–8]: It is indeed a clear advantage to use a well-established growth technique that leads to very high optical quality of the materials. However, InAs/GaAs QDs, self-assembled via Stranski-Krastanov, show a low aspect ratio whose control is rather complex to achieve,[15] due to the details of the mechanism of strain relaxation that leads to QD self-nucleation. The low aspect ratio introduces a large number of excited states into the system compared to the ideal situation of a cubic/spherical QD, which can couple with the barrier states and increase thermal or tunneling escape from the QDs. This mechanism is clearly competitive with the optical extraction of carriers from the QDs that constitute the IB states, and can be one of the causes of the pinning of the Fermi level to the IB, that leads to the decrease of open circuit voltage in QD devices. That implies the careful design the QD states, not only of the ground state, which defines the absorption threshold, but rather of the entire energy density of states of the QDs. This strategy, and in particular the increase of the ground to first excited state transition energy,[16] obtained by growing small and raised QD geometries, permits the creation of an IB that is energetically isolated from the conduction band (CB) and reaches the objectives of IB regime operation and high device open circuit voltage without the need for additional wider band gap barrier layers.[14]

Going further in this direction, the possibility to tune the size of the QDs, as well as their aspect ratio, having a direct and important impact on the QD energy density of states, would provide fundamental degree of freedom in the quantum design of the IB solar cells.

Droplet epitaxy (DE) is a growth method which allows the self-assembly of QDs of high density[17,18] and good optical quality[19] with materials of the same lattice parameter, thus avoiding strain-related defectivity and enabling the realization of QDs with a full and independent control of the nanostructure shape and size.[20] In addition, the capability of DE to realize QDs without the presence of a wetting layer at the base of the QD, a typical characteristic of the InAs/GaAs QDs, also allows the study of a pure QD system, with the IB made up of three-dimensionally confined states only.[21,22]

Leveraging on the extremely flexible shape control permitted by DE for the QD self-assembling, here, we extend the concepts of IB-CB decoupling by quantum design of the dot states[16] through the fine tuning of the QD electronic density of states. QDs with controlled size and aspect ratios are investigated, thus allowing the independent control of the position of the IB inside the bandgap of $Al_{0.3}Ga_{0.7}As$ and of the energy gap between the ground state and the excited states of the QDs. This makes possible to highlight the independent role played by the ground state energy and the structure of the energy density of states of the QDs in the temperature stability of the two-photon absorption and open circuit voltage preservation.

2 | EXPERIMENTAL

The devices were grown by conventional solid-source molecular beam epitaxy (MBE) on standard 2-in. n-doped GaAs wafers.

The QD layer was introduced in the intrinsic region of the PIN $Al_{0.3}Ga_{0.7}As$ diode, 100 nm above the n-type base layer. The QDs were grown by DE, depositing 4 (SA series) and 3 (SB series) monolayers (ML) of Ga at 180°C, followed by annealing in As atmosphere at 350°C. The QDs were capped with $Al_{0.3}Ga_{0.7}As$ grown by migration enhanced epitaxy at 350°C. All the other layers in the structure were grown at 650°C. The QDs were delta-doped with a Si pulse to have one donor per dot, thus half-filling the IB.

A sample with identical growth steps, including temperature changes and switching of molecular beams, but without the deposition of the Ga droplets, was grown as a reference sample. After the growth, all the samples were annealed ex situ at 750°C for 4 min with a conventional RTA system in nitrogen atmosphere, using a GaAs wafer as a proximity cap to minimize the desorption of As from the surface. The annealing has been already shown to improve the intensity of photoluminescence (PL) of GaAs/AlGaAs QDs,[23,24] related to a reduction of parasite non-radiative recombination mechanisms. This is of course beneficial in solar cells too because an increased optical quality of the material translates into devices closer to the radiative limit. Finally, a front contact grid of Ti/Pt/Au was evaporated on the top of the samples, followed by back contact metallization with Ni/Au/Ge/Au. The contact metals were annealed in 420°C. Contact GaAs layer was removed by wet etching prior to the deposition of double layer (TiO_2/SiO_2) antireflection coating using electron beam evaporator.

An additional sample series for morphological measurement was fabricated with the same growth conditions but stopping the growth after the QD formation.

Single devices were isolated on the wafer by conventional photolithography and wet chemical etching.

The size and density of the nanostructures were measured by atomic force microscopy (AFM) working in tapping mode with 2-nm resolution tip. The spectroscopic characterization was performed by means of the ensemble PL. The sample was excited above the barrier bandgap by focusing the 532-nm line from a Nd:YAG continuous wave (CW) laser on a spot with a diameter of approximately 100 μm. The PL signal was dispersed by a 150 g/mm diffraction grating in a

500-mm focal length spectrometer and finally detected by a Peltier-cooled charge-coupled device (CCD).

The photoresponse of the devices was measured using a single monochromatic beam setup: A halogen light source is used to provide monochromatic light through a Czerny-Turner single pass grating monochromator, with order sorting filters, and a chopper is used to modulate the intensity. The alternate electric signal is collected by a low noise transimpedance preamplifier that keeps the solar cells biased at 0 V and finally demodulated by a lock-in amplifier and digitalized. The intensity of the light beam is measured using a calibrated Si photodiode, to calculate the quantum efficiency of the devices under test. No extended light bias was applied during the measurements, to avoid unwanted population of states by the sub-gap components of the bias light. A similar setup is used for temperature dependent measurements, with the samples placed in a closed cycle He cryostat: The signal is collected through twisted and shielded wires wrapped around the cold finger of the cryostat, to reduce the noise. The sample is electrically isolated from the ground of the cryostat. A second window of sapphire in the cryostat was available to illuminate the solar cell with sub-gap light and excite double photon photocurrent, as described in Canovas et al,[25] down to about 6 μm in wavelength. A different window of ZnSe, providing transparency down to about 20 μm, has been tested, but results were identical to the sapphire window. The secondary beam was provided by a calibrated tungsten filament filtered with a polished Ge wafer and focused onto the sample with two spherical mirrors or by an attenuated 1064-nm Nd:YAG laser coupled with a beam expander to achieve similar power density.

3 | RESULTS AND DISCUSSION

The AFM topography of uncapped SA and SB samples is reported in Figure 1. The number density of the nanostructures is $\approx 4 \cdot 10^{10}$ cm^{-2} in both cases. The average QD height is 6.6 and 3 nm for samples A and B, respectively. The average base size is ≈25 nm with a distribution full width half maximum of 5 nm in both samples. The calculated average aspect ratio is therefore $\rho = 0.26$ (SA) and $\rho = 0.12$ (SB). The observed control over QD shape and number density is related to the peculiarities of the droplet density QD self-assembly procedure. In the DE, each QD develops, during the annealing in As atmosphere, from a previously deposited droplet. The droplet density is determined by the Ga deposition parameters, namely, substrate temperature and Ga deposition rate.[26,27] Being such parameters identical, for both sample types, during the droplet deposition step, the resulting droplet density (and in turn the QD density) is the same. For what concerns the QD base size, it is determined by the conditions during the annealing of the droplet in As atmosphere.[20] Also in this case, being the annealing condition equal for both samples, the QD base is the same. On the other side, a marked dependence of the QD height on the droplet volume, other growth conditions being equal, has been observed.[20] We therefore used this dependence to control the aspect ratio in our samples.

The low temperature (T = 15 K) PL spectra of the samples are characterized by a broad band, of ≈100 meV, peaked at 1.67 eV (SA) and 1.80 eV (SB), respectively (Figure 2). To correlate the QD emission with the actual QD shape, we performed numerical calculations of the QD energy levels. To compute the band structure, we

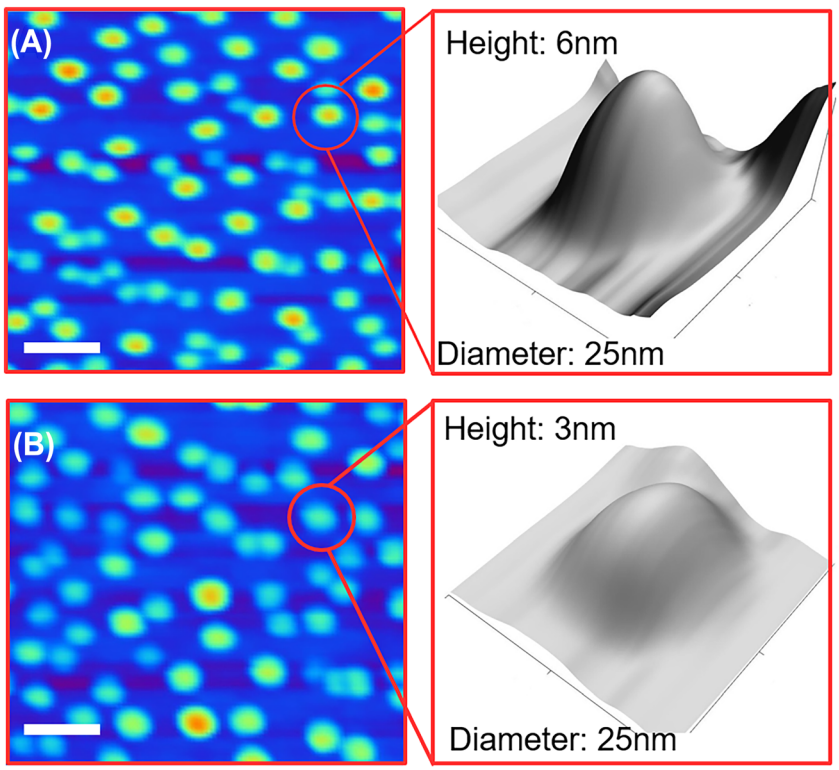

FIGURE 1 AFM images of uncapped samples. Left panels: top view of the samples (500 × 500 nm^2) of SA (A) and SB (B). The white bars indicate 100-nm length. The average density in both samples is 4 × 10^{10}/cm^2. Right panels: 3D view of the highlighted QD in SA (A) and SB (B). The average dot base is 25 nm in both samples, while the dot height is 6 and 3 nm in SA and SB, respectively. [Colour figure can be viewed at wileyonlinelibrary.com]

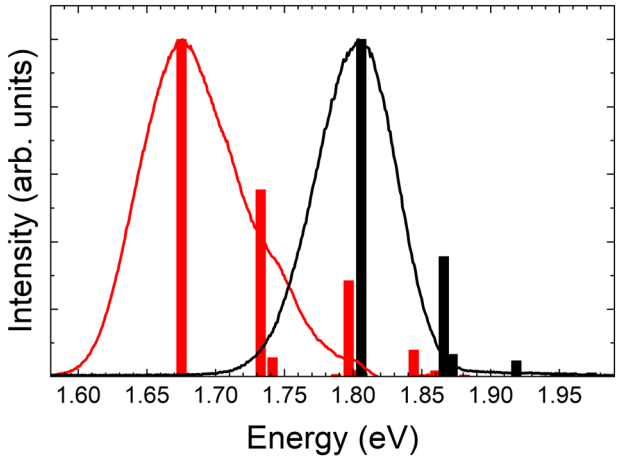

FIGURE 2 Normalized photoluminescence spectra, measured at T = 15 K, of SA (red line) and SB (black line), respectively. The transition probabilities, calculated based on the AFM measured shape of the QDs, are reported as red (SA) and black (SB) histograms. The height of the histograms is proportional to the optical strength of the transition. [Colour figure can be viewed at wileyonlinelibrary.com]

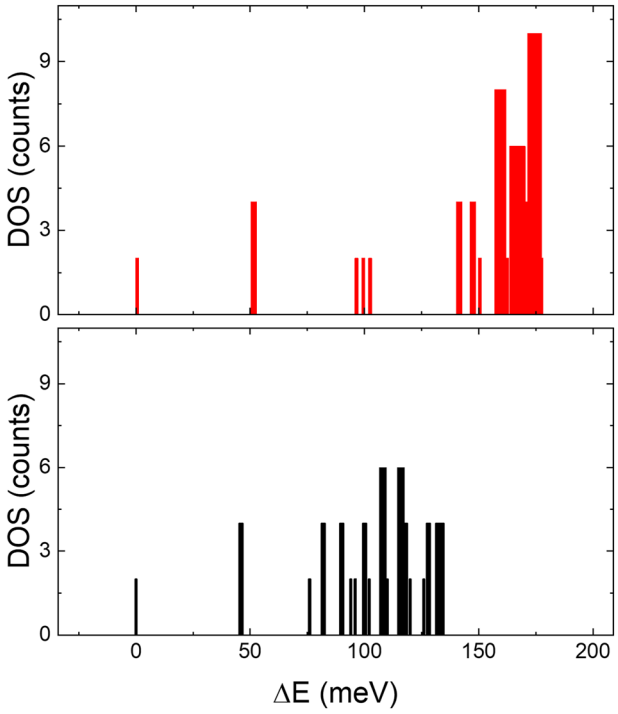

FIGURE 3 Calculated electron density of states (energies are reported as differences with respect to the QD ground state) for SA (red) and SB (black) QDs. [Colour figure can be viewed at wileyonlinelibrary.com]

solved the single-electron drift-diffusion equations including Pikus–Bir strain corrections. The confined energy states were then computed based on the envelope function approximation with an eight band k·p model. Materials parameters were taken from Vurgaftman et al.[28] The QD shape is assumed to be a truncated cone[20] with height and width as obtained from the AFM analysis. In order to take into account the transition probability, we computed the optical matrix element of the different transitions. This is defined as the matrix element between the final state and the initial with the momentum operator, which considers the interaction of carriers with photons. The shape of the QDs was defined based on the analysis of the AFM image shown in Figure 1. This is made possible by the small interdiffusion of group III species in GaAs/AlGaAs QDs during capping.[29] Our numerical calculations confirm that the difference in the observed spectra can be totally attributed to the different electronic states induced by the change in the aspect ratio between SA and SB. The calculated ground state transition energies, 1.68 eV for sample A and 1.80 eV for sample B, well reproduce the observed peaks (see Figure 2). Figure 2 also reports the histogram of the calculated QD transition optical matrix elements. From the comparison with the PL spectra, the two shoulder peaks of sample SA emitting at 1.74 and 1.80 eV can be attributed to the emission from the excited states, coinciding with the values of the first and second excited electron–hole transitions. The calculated electron density of states is reported in Figure 3. The ground to first excited state energy separation, owing to the similar QD radius of SA and SB, is ≈50 meV, thus effectively decoupling the QD ground state from the excited states. In sample A, owing to its high aspect ratio, the energy separation of about 50 meV is maintained up to the third confined QD state, while in sample B, a sizeable density of states, with energy separation close to the LO phonon energy ($\hbar\omega_{LO} = 36$ meV) from the first excited state, is present (see Figure 3). As a matter of fact, the phonon density of states is not affected by the presence of small QDs,[30] so bulk properties can be used for the electronic state design.

The observation (Figure 3) of well-isolated excited states in the QD electronic density of states, from the operating principle perspective, does not impact on the maximum theoretical efficiency of the IB solar cell. In terms of actual devices, having several isolated IBs could help to harvest a broader portion of the sun spectrum.[10,11,31]

The formation of QD minibands is suppressed in our samples along the growth direction due to the presence of a single QD layer. In the QD plane, the lateral coupling at densities lower than 10^{11} cm^{-2} is negligible also because, in contrast to self-assembled Stranski–Krastanov QDs where the wetting layer mediates the coupling,[32] we suppressed the wetting layer formation in our DE-QDs. The latter choice has been done to decrease the thermal escape probability of the carriers in the QDs.[33,34] As a matter of fact, the operating principle of the QD-based IB solar cell does not require the formation of a miniband through the vertical or lateral coupling of QD states.[35]

The external quantum efficiency (EQE) of the devices has been measured at room temperature without the application of any optical bias apart from the monochromatic light. The results, reported in Figure 4, clearly show that the photoresponse is extended below the bandgap of $Al_{0.3}Ga_{0.7}As$ in the samples containing QDs. This is due to the introduction of the QD states into the energy gap of the barrier that can be tuned by changing the QD aspect ratio. This aspect ratio effect can be clearly detected comparing the QD samples in the graph: the onset of the photoresponse changes from 1.51 eV for the

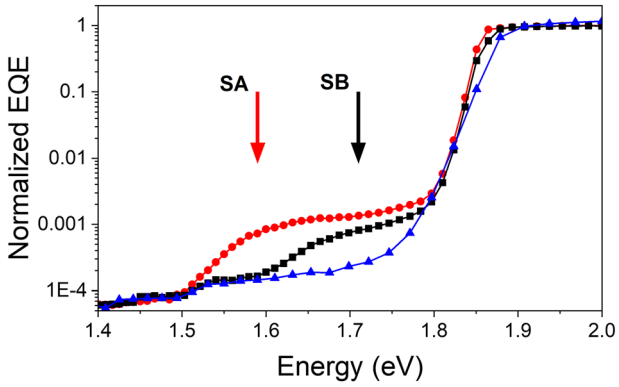

FIGURE 4 Normalized EQE, measured at room temperature of the QD solar cells, compared to the reference device (no QDs). Three different photocurrent production thresholds are clearly detectable that we attribute to the VB-CB transitions (ref. sample, blue) and to the VB-IB transitions of SA (red curve) and SB (black curve). The calculated ground state transitions, translated by 90 meV, are indicated by the red (SA) and black (SB) arrows. [Colour figure can be viewed at wileyonlinelibrary.com]

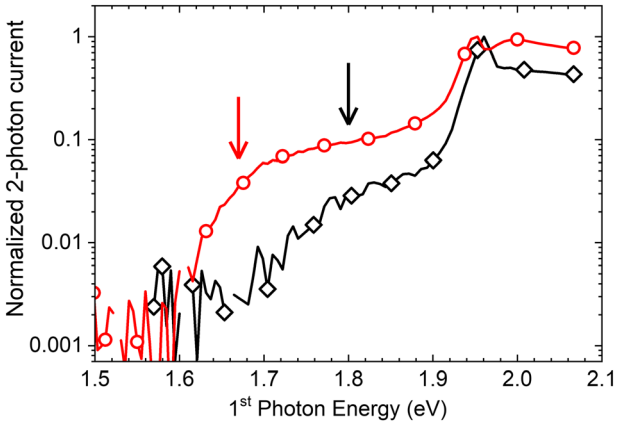

FIGURE 5 Two-photon photocurrent of the quantum dot solar cells from SA (red curve) and SB (black curve), clearly showing the effect of the QD aspect ratio in the shift of the position of the intermediate band absorption. The red and black arrows indicate the energy peak of the PL from SA and SB, respectively. The peak at 1.95 eV is attributed to excitonic absorption from the AlGaAs barrier, that is, slightly shifted in the two samples due to a little variation of the Al molar fraction in the alloy. [Colour figure can be viewed at wileyonlinelibrary.com]

large dots to 1.61 eV for the small ones. The transitions observed in the device photocurrent are in very good agreement with the recombination transitions measured by PL (Figure 2), provided that the 90-meV red shift of the GaAs gap is taken into account due to the temperature difference between the PL (T = 15 K) and the EQE (T = 300 K) measurement temperatures. The PL emission from the fundamental QD states begins at about 1.60 and 1.72 eV for large (SA) and small (SB) QD, respectively, due to the size dispersion. Compared to the solar cell photocurrent generation threshold, this means that the larger dots within the ensembles are responsible for the rise of the photoresponse at 1.51 (SA) and 1.61 eV (SB).

A two-photon photocurrent measurement experiment was set up following Canovas et al,[25] in order to measure the capability of our QD devices to convert radiation below the bandgap of the AlGaAs barrier and to pump electrons in the CB of the barrier. A more extensive description of this experiment has been given elsewhere.[36] The nanostructured solar cells clearly show two-photon photocurrent with sub-gap excitation (Figure 5). The results are the same using a filtered hot filament or a 1064-nm laser for the below bandgap excitation of the QD band, provided that the same power is delivered to the devices.

As shown in Figure 5, the onsets of the two-photon signals match well the onsets of the single-photon photoresponse measurements reported in Figure 4, considering a blue shift of about 90 meV due to the temperature measurement difference. We interpret the photocurrent signal detected at energies of the monochromatic beam (primary) above the bandgap of $Al_{0.3}Ga_{0.7}As$ ($E_{gap} \approx 1.97$ eV) as coming from charge carriers generated in the barrier, captured by QDs, excited as free carriers by the IR sub-gap beam (secondary) and eventually collected. When the primary beam is not provided, no signal is detected, proving that the signal comes from transitions induced by the photons injected by the primary beam excitation.

The peaks at 1.95 eV are due to the exciton absorption peak of $Al_{0.3}Ga_{0.7}As$; the small variation of about 5 meV in the peak energy is compatible with the usual fluctuations in Al content in MBE samples. Since no wetting layer is grown by DE in the conditions used to grow our samples, we exclude the possibility that this peak originates from quantum well-like states. For energies of the primary beam below the bandgap of the host, we can observe a decay of the signal to the noise level of the experiment, a few picoamps, at about 1.6 and 1.7 eV for sample B and A, respectively. This is not only consistent with the single photon photoresponse at room temperature but also with the PL spectra of the two samples, shown in Figure 2. The differences between the two samples are due to the different sizes of the QDs, showing for the first time that it is possible to tune the energy levels of the IB in this kind of solar cells. As it was shown in a previous letter,[36] no two-photon photocurrent signal is detected above noise level in reference samples grown with identical structure and temperature but lacking the QD nucleation step.

As it is well known, the PL energy peaks are associated with transitions of electrons from the fundamental confined state in the QD CB to its analogous in the QD valence band. This of course means that for recombination to take place, both an electron and a hole must be spatially localized in the same QD, for non-interacting dots at least. The reverse process, optical generation of carriers by sub-gap light directly inside the QDs, populates the dots with both electrons and holes.

To investigate the optical extraction process of carriers from the QDs, we performed photocurrent measurements in the two-photon configuration at different temperatures, up to 175 K, where the signal level becomes too low to be clearly identified above the noise. The above-gap contribution, including the excitonic peak, was subtracted

from the curve and the remaining part, that is the QD-only contribution, and was integrated for all the temperatures. In this way, we exclude the above-gap absorption, dot capture, and re-emission processes from the analysis. The normalized data are shown in form of Arrhenius plot in Figure 6. It is evident how the slope at high temperatures is different between the two samples, suggesting a different activation energy for the mechanisms of thermal quenching of the two-photon signal. The curve is interpolated with the following function:

$$I = \frac{I_0}{1 + C \cdot e^{-E_a/kT}}$$

The results of the fit for the two curves are activation energies of 88 ± 6 and 39 ± 2 meV, for the SA and SB devices, respectively.

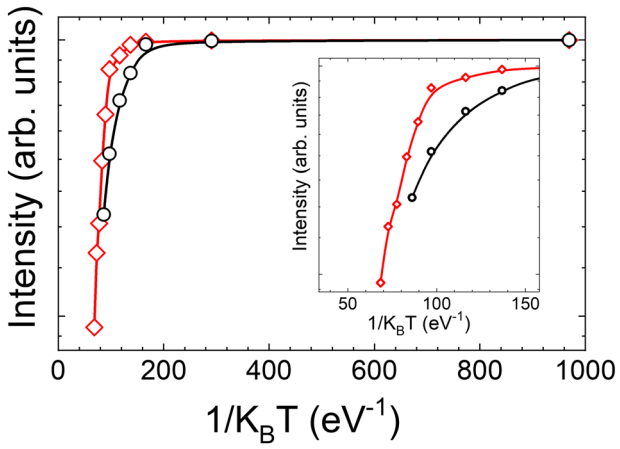

FIGURE 6 Arrhenius plot of the two-photon photocurrent intensity for excitation below the bandgap of AlGaAs of SA (red curve) and SB (black curve). The slope at high temperature is also reported as inset. [Colour figure can be viewed at wileyonlinelibrary.com]

Despite the dynamics of the fitted signal is too low for the results to be accurate, the fit gives another indication that the process of optical extraction involves deeper levels in the case of bigger QDs. Since for an IB solar cell to work efficiently, one would require that the optical extraction process is dominant over the thermal extraction (that does not preserve the output voltage), a large activation energy for thermal quenching is needed.

The signal detected in the two-photon experiment comes from the contribution of all the QDs excited by the sub-gap photons; this means that for a given QD ensemble with its size spread, contributions from small dots, with relatively shallow fundamental confined energy levels, will be quenched at lower temperature than contributions from larger dots, with deeper fundamental levels. Not only, since the size spread translates into a spread in the dot energy levels, at high primary beam energies (though still below gap), we can expect contributions from all the dots in the ensemble, while at low energies, only the bigger dots can contribute to the absorption. For this reason, the activation energies extracted from the fit of the experimental data should not be interpreted directly as the depth of the fundamental levels, which are of the order of 200 meV. The results of the fit are an average of the response of different dot sizes present in each sample and of the interaction of sub-gap photons with their ground and excited states. In fact, larger dots also show confined excited states, which can be either thermally or optically populated (by the primary beam): The secondary beam can thus extract carriers from states that are shallower than the ground state of the dots and contribute to the detected signal.

The higher temperature visibility of the two-photon absorption process in sample A with respect to sample B calls for a reduction of the effects of the pinning of the quasi-Fermi electronic level on the QD ground states. According to the models describing the transition processes in QDs via polaron excitations,[37] the phonon assisted transition probability between confined states decreases by orders of magnitude when the energy separation ΔE between the initial and

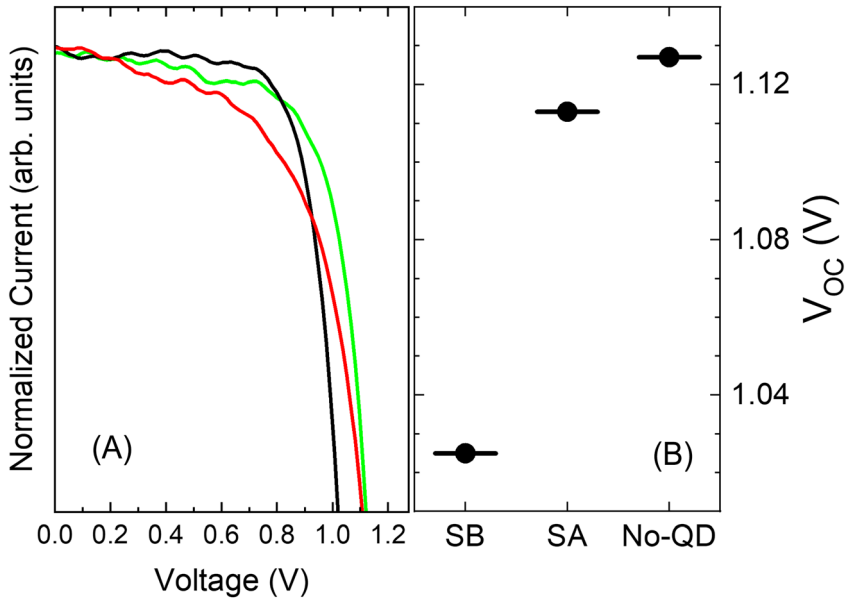

FIGURE 7 (a) I–V curve of the SA (red), SB (black), and AlGaAs without QD (green) cells. (b) Open circuit voltage V_{OC} of the fabricated photovoltaic cells SA, SB, and the AlGaAs cell fabricated without the QDs. [Colour figure can be viewed at wileyonlinelibrary.com]

final states is strongly detuned from a multiple of the longitudinal optical (LO) phonon energy ($\Delta E \neq n\hbar\omega_{LO}$, where n is an integer). This suggests that, being in both samples SA and SB the ground to first excited energy separation large ($\Delta E \approx 50$ meV) and detuned from $\hbar\omega_{LO}$, the phonon assisted transition process is quenched. For this reason, we expect the two quasi-Fermi levels of the IB and CB in both samples well separate even at high temperatures, due to the suppression of phonon assisted processes, thus improving the performance of the IB solar cell. The $\hbar\omega_{LO}$ energy detuning is more effective in sample SA, where the density of states is maintained delta-like and with large energy gaps up to the third excited quantum confined state (see Figure 3).

The expected separation between the IB and CB Fermi energy levels obtained by the engineering of the QD states has a direct consequence on the open circuit voltage V_{OC} of the cells at room temperature. In Figure 7, we report the I–V curves at one sun of cells SA and SB compared to that of an AlGaAs reference cell. The insertion of a layer of QDs in the structure degrades the V_{OC} of both SA and SB cells. Despite that, both the SA and SB cells show a moderate degradation of the V_{OC}, being $\Delta V_{OC} \approx 100$ mV in SB cell and only $\Delta V_{OC} = 14$ mV in SA cell.[2] We attribute such low values to the careful detuning of the ground to excited state energy difference from the $\hbar\omega_{LO}$ energy. In addition, the V_{OC} reduction, attributed to the coupling of the IB and CB Fermi energies, is extremely small in the SA cell, despite an IB ground state energy lying 180 meV below the CB. Apparently, the observed behavior seems to go in the opposite direction from the findings of Beattie et al.[16] There, the cell with the larger QDs, those with a lower ground state energy, had the poorest V_{OC} preservation. Here, sample SA electronic structure was designed to maximize at the same time the effect of $\hbar\omega_{LO}$ detuning, obtained by increasing the energy level separation (as in Beattie et al,[16]) to reduce the inter-level phonon transition probability, and to tune the localized density of states and the IB-CB energy difference to reduce the QD thermal escape rate.

4 | CONCLUSIONS

We have reported on the characterization of GaAs/AlGaAs QD photovoltaic cells grown by DE. This technique allows the realization of lattice matched nanostructures without the presence of wetting layers and relief of strain by introduction of dislocations in the epitaxial film. We exploited the capability to control the actual shape of the QDs to show that it is possible to finely tune the electronic states of the QDs to (1) decrease the sub-gap absorption wavelength threshold in IB solar cells, for a better spectral match with sunlight; and (2) engineer the thermalization and the extraction process of carriers from the IB by reducing the phonon assisted transition probability and increasing the thermal extraction barrier energy.

The combination of the two effects makes the photonic extraction mechanism increasingly dominant at room temperature. Consequently, we observed a reduction of the open circuit voltage of only 14 mV, compared to the reference cell.

The insertion of a single layer of QDs, although with a high number density (4×10^{10} cm^{-2}), increases negligibly the short-circuit current. Multiple layers of dots need to be stacked to achieve significant sub-gap absorption, and this is feasible in principle, since the GaAs/AlGaAs system is strain-free, without the introduction of crystal defects. Moreover, light-trapping techniques can be exploited to further increase first and second photon optical transitions, increasing the short-circuit current and preserving the open circuit voltage thanks to the improved ratio between optical and thermal extraction rates from the IB.[31,38,39]

AUTHOR CONTRIBUTIONS

Andrea Scaccabarozzi, Stefano Vichi, Sergio Bietti, Maurizio Acciarri, Federica Cappelluti and Stefano Sanguinetti conceived and designed the experiments. Sergio Bietti grew the samples. Andrea Scaccabarozzi and Timo Aho processed the samples and performed the experiments. Federico Cesura performed the morphological measurements. Stefano Vichi made the quantum simulations. All authors discussed the results and wrote the manuscript.

ACKNOWLEDGEMENTS

Federica Cappelluti, Timo Aho, and Mircea Guina acknowledge partial support from European Union Horizon 2020 project TFQD (Grant Agreement No. 687253). Open Access Funding provided by Universita degli Studi di Milano-Bicocca within the CRUI-CARE Agreement.

[Correction added on 17 February 2023, after first online publication: Author Contributions and Acknowledgements have been corrected in this version.]

CONFLICT OF INTEREST STATEMENT

The authors declare no conflicts of interest.

DATA AVAILABILITY STATEMENT

The data that support the findings of this study are available from the corresponding author upon reasonable request.

ORCID

Federica Cappelluti https://orcid.org/0000-0003-4485-9055

Stefano Sanguinetti https://orcid.org/0000-0002-4025-2080

REFERENCES

1. Luque A, Marti A. Increasing the efficiency of ideal solar cells by photon induced transitions at intermediate levels. *Phys Rev Lett*. 1997; 78(26):5014-5017. doi:10.1103/PhysRevLett.78.5014
2. Okada Y, Ekins-Daukes NJ, Kita T, et al. Intermediate band solar cells: recent progress and future directions. *Appl Phys Rev*. 2015;2(2): 021302. doi:10.1063/1.4916561
3. Luque A, Marti A, Antolin E, Tablero C. Intermediate bands versus levels in non-radiative recombination. *Phys B*. 2006;382(1-2):320-327. doi:10.1016/j.physb.2006.03.006
4. Marti A, Antolin E, Stanley C, et al. Production of photocurrent due to intermediate-to-conduction-band transitions: a demonstration of a key operating principle of the intermediate-band solar cell. *Phys Rev Lett*. 2006;97:1.
5. Sablon KA, Little JW, Mitin V, Sergeev A, Vagidov N, Reinhardt K. Strong enhancement of solar cell efficiency due to quantum dots with

built-in charge. *Nano Lett*. 2011;11(2311):2311-2317. doi:10.1021/nl200543v
6. Sugaya T, Kamikawa Y, Furue S, Amano T, Mori M, Niki S. Multi-stacked quantum dot solar cells fabricated by intermittent deposition of InGaAs. *Sol Energy Mater sol Cells*. 2011;95(1):163-166. doi:10.1016/j.solmat.2010.04.040
7. Tutu FK, Sellers IR, Peinado MG, et al. Improved performance of multilayer InAs/GaAs quantum-dot solar cells using a high-growth-temperature GaAs spacer layer. *J Appl Phys*. 2012;111(4):046101. doi:10.1063/1.3686184
8. Wu J, Makableh YFM, Vasan R, et al. Strong interband transitions in InAs quantum dots solar cell. *Appl Phys Lett*. 2012;100(5):051907. doi:10.1063/1.3681360
9. Marti A, Lopez N, Antolin E, et al. Emitter degradation in quantum dot intermediate band solar cells. *Appl Phys Lett*. 2007;90(23):233510. doi:10.1063/1.2747195
10. Gioannini M, Cedola AP, Di Santo N, Bertazzi F, Cappelluti F. Simulation of quantum dot solar cells including carrier Intersubband dynamics and transport. *IEEE J Photovoltaics*. 2013;3(4):1271-1278. doi:10.1109/JPHOTOV.2013.2270345
11. Cappelluti F, Tukiainen A, Aho T, et al. Quantum dot-based thin-film III–V solar cells. In: P Y, Wang Z, eds. *Quantum Dot Optoelectronic Devices. Lecture Notes in Nanoscale Science and Technology*. Berlin: Springer; 2020.
12. Luque A, Marti A, Lopez N, et al. Experimental analysis of the quasi-Fermi level Split in quantum dot intermediate-band solar cells. *Appl Phys Lett*. 2005;87(8):083505. doi:10.1063/1.2034090
13. Marti A, Lopez N, Antolin E, et al. Novel semiconductor solar cell structures: the quantum dot intermediate band solar cell. *Thin Solid Films*. 2006;511–512:638.
14. Abouelsaood AA, Ghannam MY, Poortmans J. On the reported experimental evidence for the quasi-Fermi level split in quantum-dot intermediate-band solar cells. *Prog Photovolt Res Appl*. 2013;21(2):209-216. doi:10.1002/pip.1192
15. Kaizu T, Matsumura T, Kita T. Broadband control of emission wavelength of InAs/GaAs quantum dots by GaAs capping temperature. *J Appl Phys*. 2015;118(15):154301. doi:10.1063/1.4933182
16. Beattie NS, See P, Zoppi G, et al. Quantum engineering of InAs/GaAs quantum dot based intermediate band solar cells. *ACS Photonics*. 2017;4(11):2745-2750. doi:10.1021/acsphotonics.7b00673
17. Jo M, Mano T, Sakuma Y, Sakoda K. Extremely high-density GaAs quantum dots grown by droplet epitaxy extremely high-density GaAs quantum dots grown by droplet epitaxy. *Appl Phys Lett*. 2012;100(21):212113. doi:10.1063/1.4721663
18. Kim JS, Jeong MS, Byeon CC, et al. GaAs quantum dots with a high density on a GaAs (111)a substrate. *Appl Phys Lett*. 2006;88(24):241911. doi:10.1063/1.2213012
19. Basso Basset F, Bietti S, Reindl M, et al. High-yield fabrication of entangled photon emitters for hybrid quantum networking using high-temperature droplet epitaxy. *Nano Lett*. 2018;18(1):505-512. doi:10.1021/acs.nanolett.7b04472
20. Bietti S, Bocquel J, Adorno S, et al. Precise shape engineering of epitaxial quantum dots by growth kinetics. *Phys Rev B*. 2015;92(7):075425. doi:10.1103/PhysRevB.92.075425
21. Sanguinetti S, Watanabe K, Tateno T, et al. Role of the wetting layer in the carrier relaxation in quantum dots. *Appl Phys Lett*. 2002;81(4):613-615. doi:10.1063/1.1495525
22. Sanguinetti S, Watanabe K, Tateno T, et al. Modified droplet epitaxy GaAs/AlGaAs quantum dots grown on a variable thickness wetting layer. *J Cryst Growth*. 2003;253(1-4):71-76. doi:10.1016/S0022-0248(03)01016-9
23. Sanguinetti S, Mano T, Gerosa A, et al. Rapid thermal annealing effects on self-assembled quantum dot and quantum ring structures. *J Appl Phys*. 2008;104(11):113519. doi:10.1063/1.3039802
24. Sanguinetti S, Watanabe K, Kuroda T, Minami F, Gotoh Y, Koguchi N. Effects of post-growth annealing on the optical properties of self-assembled GaAs/AlGaAs quantum dots. *J Cryst Growth*. 2002;242(3-4):321-331. doi:10.1016/S0022-0248(02)01434-3
25. Canovas E, Marti A, Lopez N, et al. Low temperature characterization of the photocurrent produced by two-photon transitions in a quantum dot intermediate band solar cell. *Thin Solid Films*. 2008;516(20):6919-6923. doi:10.1016/j.tsf.2007.12.061
26. Ratsch C, Venables JA. Nucleation theory and the early stages of thin film growth. *J Vac Sci Technol a Vacuum, Surfaces, Film*. 2003;21:S96.
27. Heyn C, Stemmann A, Schramm A, Welsch H, Hansen W, Nemcsics Á. Regimes of GaAs quantum dot self-assembly by droplet epitaxy. *Phys Rev B*. 2007;76(7):075317. doi:10.1103/PhysRevB.76.075317
28. Vurgaftman I, Meyer JR, Ram-Mohan LR. Band parameters for {III}-V compound semiconductors and their alloys. *J Appl Phys*. 2001;89(11):5815-5875. doi:10.1063/1.1368156
29. Keizer JG, Bozkurt M, Bocquel J, et al. Shape control of quantum dots studied by cross-sectional scanning tunneling microscopy. *J Appl Phys*. 2011;109(10):102413. doi:10.1063/1.3577960
30. Vanacore GM, Hu J, Liang W, Bietti S, Sanguinetti S, Zewail AH. Di Ff Raction of quantum dots reveals nanoscale ultrafast energy localization. *Nano Lett*. 2014;14(11):6148-6154. doi:10.1021/nl502293a
31. Mellor A, Luque A, Tobías I, Martí A. The feasibility of high-efficiency InAs/GaAs quantum dot intermediate band solar cells. *Sol Energy Mater sol Cells*. 2014;130:225-233. doi:10.1016/j.solmat.2014.07.006
32. Cornet C, Platz C, Caroff P, et al. Approach to wetting-layer-assisted lateral coupling of InAs InP quantum dots. *Phys Rev B - Condens Matter Mater Phys*. 2005;72(3):035342. doi:10.1103/PhysRevB.72.035342
33. Sanguinetti S, Henini M, Grassi Alessi M, Capizzi M, Frigeri P, Franchi S. Carrier thermal escape and retrapping in self-assembled quantum dots. *Phys Rev B*. 1999;60(11):8276-8283. doi:10.1103/PhysRevB.60.8276
34. Sanguinetti S, Mano T, Oshima M, Tateno T, Wakaki M, Koguchi N. Temperature dependence of the photoluminescence of InGaAs/GaAs quantum dot structures without wetting layer. *Appl Phys Lett*. 2002;81(16):3067-3069. doi:10.1063/1.1516632
35. Ramiro I, Martí A. Intermediate band solar cells: present and future. *Prog Photovoltaics Res Appl*. 2021;29(7):705-713. doi:10.1002/pip.3351
36. Scaccabarozzi A, Adorno S, Bietti S, Acciarri M, Sanguinetti S. Evidence of two-photon absorption in strain-free quantum dot GaAs/AlGaAs solar cells. *Phys Status Solidi Rapid Res Lett*. 2013;7(3):173-176. doi:10.1002/pssr.201206518
37. Steinhoff A, Kurtze H, Gartner P, et al. Combined influence of coulomb interaction and polarons on the carrier dynamics in InGaAs quantum dots. *Phys Rev B*. 2013;88(20):205309. doi:10.1103/PhysRevB.88.205309
38. Aho T, Guina M, Elsehrawy F, et al. Comparison of metal/polymer back reflectors with half-sphere, blazed, and pyramid gratings for light trapping in III-V solar cells. *Opt Express*. 2018;26(6):A331-A340. doi:10.1364/OE.26.00A331
39. Elsehrawy F, Niemi T, Cappelluti F. Guided-mode resonance gratings for intermediate band quantum dot solar cells. *Opt Express*. 2018;26(6):A352-A359. doi:10.1364/OE.26.00A352

How to cite this article: Scaccabarozzi A, Vichi S, Bietti S, et al. Enhancing intermediate band solar cell performances through quantum engineering of dot states by droplet epitaxy. *Prog Photovolt Res Appl*. 2023;1-8. doi:10.1002/pip.3672